Biointerphases

RESEARCH ARTICLE | APRIL 11 2023

Insight into the assembly of lipid-hyaluronan complexes in osteoarthritic conditions

Special Collection: Special Topic Collection: Polymeric Biointerfaces — A Collection in celebration of Nicholas D. Spencer's career

Kangdi Sun ; Tooba Shoaib ; Mark W. Rutland ; Joesph Beller ; Changwoo Do ; Rosa M. Espinosa-Marzal

Check for updates

Biointerphases 18, 021005 (2023)
https://doi.org/10.1116/6.0002502
CHORUS

View Online
Export Citation

13 May 2024 08:52:55

Biophysics Reviews
Call for Applicants
Seeking New Editor-in-Chief
AIP Publishing

Biointerphases
A Journal of Biomaterials and Biological Interfaces

ARTICLE

avs.scitation.org/journal/bip

Insight into the assembly of lipid-hyaluronan complexes in osteoarthritic conditions

Cite as: Biointerphases 18, 021005 (2023); doi: 10.1116/6.0002502
Submitted: 19 January 2023 · Accepted: 28 February 2023 ·
Published Online: 11 April 2023

View Online Export Citation CrossMark

Kangdi Sun,[1,a)] Tooba Shoaib,[2,a)] Mark W. Rutland,[3] Joesph Beller,[4,b)] Changwoo Do,[2,c)] and Rosa M. Espinosa-Marzal[1,5,c)]

AFFILIATIONS

[1]Materials Science and Engineering Department, University of Illinois at Urbana-Champaign, Urbana, Illinois 61801
[2]Neutron Scattering Division, Oak Ridge National Laboratory, Oak Ridge, Tennessee 37830
[3]KTH Royal Institute of Technology, Department of Chemistry, Stockholm SE-100 44, Sweden; School of Chemistry, University of New South Wales, Sydney 2052, Australia; Laboratoire de Tribologie et Dynamique des Systèmes, École Centrale de Lyon, Lyon 69130, France; and Bioeconomy and Health, Materials and Surface Design, RISE Research Institutes of Sweden, Stockholm, Sweden
[4]University of Tennessee, Knoxville, Tennessee 37996
[5]Civil and Environmental Engineering Department, University of Illinois at Urbana-Champaign, Urbana, Illinois 61801

Note: This paper is part of the Biointerphases Special Topic Collection on Polymeric Biointerfaces A collection in celebration of Nicholas D. Spencers career.

[a)]First co-authors.
[b)]**Email:** josdbell@vols.utk.edu
[c)]**Authors to whom correspondence should be addressed:** doc1@ornl.gov and rosae@illinois.edu

13 May 2024 08:52:55

ABSTRACT

Interactions between molecules in the synovial fluid and the cartilage surface may play a vital role in the formation of adsorbed films that contribute to the low friction of cartilage boundary lubrication. Osteoarthritis (OA) is the most common degenerative joint disease. Previous studies have shown that in OA-diseased joints, hyaluronan (HA) not only breaks down resulting in a much lower molecular weight (MW), but also its concentration is reduced ten times. Here, we have investigated the structural changes of lipid-HA complexes as a function of HA concentration and MW to simulate the physiologically relevant conditions that exist in healthy and diseased joints. Small angle neutron scattering and dynamic light scattering were used to determine the structure of HA-lipid vesicles in bulk solution, while a combination of atomic force microscopy and quartz crystal microbalance was applied to study their assembly on a gold surface. We infer a significant influence of both MW and HA concentrations on the structure of HA-lipid complexes in bulk and assembled on a gold surface. Our results suggest that low MW HA cannot form an amorphous layer on the gold surface, which is expected to negatively impact the mechanical integrity and longevity of the boundary layer and could contribute to the increased wear of the cartilage that has been reported in joints diseased with OA.

© 2023 Author(s). All article content, except where otherwise noted, is licensed under a Creative Commons Attribution (CC BY) license (http://creativecommons.org/licenses/by/4.0/). https://doi.org/10.1116/6.0002502

I. INTRODUCTION

The articular cartilage is one example of the many impeccable tribosystems that nature has built. It is an avascular tissue composed of chondrocytes, collagen fibers, proteoglycans, glycosaminoglycans, and elasticin.[1] The biological lubricant that provides cushioning and low friction during articulation is a viscous non-Newtonian fluid, known as the synovial fluid (SF), which contains biomolecules including hyaluronan, lubricin, and phospholipids.[2,3] Healing and repair of articular cartilage are very limited, and therefore, its preservation is paramount to joint health. Osteoarthritis (OA) is the most common degenerative joint disease. It affects around 32 million people in the U.S. alone, while more

© Author(s) 2023

than 22% of adults over 40 around the world suffer from knee OA.[4] In advanced stages, the patients suffer from severe pain, functional limitations in the affected joints, and restricted mobility. Articular cartilage undergoes significant degradation during OA.

Compositional changes of the SF are helpful in diagnosing joint diseases. For instance, analysis of the SF composition is performed if pain, inflammation, or swelling occurs in a joint, or when there is an accumulation of fluid. Analyzing the composition of SF samples can help to diagnose the exact problem causing the inflammation, which has led to active research in the diagnosis of common diseases like arthritis. This highlights that the changes in SF composition directly affect the function of the joint.[5–7] One intensively researched aspect is the synergy between biomacromolecules present in the synovia, in particular, phospholipid self-assemblies and the high molecular weight (MW) polysaccharide, hyaluronan (HA).

Phospholipids are a major component of the synovial cavity, with phosphatidylcholines (PCs) making a total of ~41% of the total lipid content. Phospholipids can self-assemble into various phases including liposomes and bilayers (or other lamellar phases) in the SF and on the cartilage's surface, respectively. Multiple mechanisms have been proposed describing the low friction coefficients in boundary lubrication provided by these self-assemblies,[8] including hydration lubrication,[9,10] reduced adhesion,[11] vesicle deformation and rupture,[12,13] as well as interbilayer sliding in the case of lamellar stacks.[14,15] It has been widely reported that phospholipids can bind with other molecules in the SF, particularly with HA, to form complexes that facilitate boundary lubrication. HA is a polysaccharide with repeating units made of glucuronic acid, and an amino sugar, linked via a glycosidic bond. While originally HA was thought to contribute toward low friction,[13] recent studies show otherwise.[16] Using a surface force balance, Klein's research group showed that its boundary lubricating ability is poor.[9] The interaction between HA and phospholipids is also widely disputed. For instance, it has been reported that HA adsorbs on the lipid or accumulates in-between lipid bilayers. In contrast, MD simulations showed that HA monomers or clusters do not adsorb on lipid bilayers.[17] This further warrants a deeper dive into the HA-lipid self-assembly and structure. The nature of the interaction between lipid and HA, and thereby, their assembly, is believed to be dependent on the MW of HA, its concentration, and solution ionic strength.[17–19] This might be associated with the ability of HA to form inter- and intra-molecular interactions depending on its MW, that is, it is difficult to form intrachain interactions in low MW HA, whereas these are easier in high MW HA.[18]

The composition of HA in the SF has been reported to significantly change during the development of OA. For a healthy joint, HA exhibits a MW of 2–20 MDa with a concentration ranging from 1 to 4 mg/ml. In the OA-diseased joints, not only is HA broken down, resulting in a much lower MW, but its concentration is also reduced by ten times.[20,21] Inspired by these results, we chose to investigate the structural changes as a function of concentration and the MW of HA to simulate the physiologically relevant conditions that exist in healthy and diseased joints. We have explored the structural properties of lipid-HA model mixtures in solution. To relate to the conditions relevant to boundary lubrication, we have also investigated the morphology and properties of the surface-adsorbed films.

II. MATERIALS AND METHODS

A. Materials

Dipalmitoylphosphatidylcholine (DPPC) in chloroform was purchased from Avanti Polar lipids (USA). Hyaluronic acid sodium salt from rooster comb, hyaluronic acid sodium salt from *Streptococcus equi* (MW 30–50 kDa), and D_2O (99.9 atom %D) were purchased from Millipore-Sigma (USA).

B. Synthesis of DPPC vesicles and HA mixtures

Unilamellar DPPC vesicles were prepared by thin film hydration followed by the standard extrusion method. Briefly, a solution of DPPC in chloroform was transferred to a round-bottom borosilicate flask and the solvent was evaporated via rotary evaporation. The dried lipid thin film was kept under vacuum overnight to ensure complete solvent removal. The lipids were rehydrated by adding NaCl buffer (in 150 mM NaCl in D_2O or H_2O) to get 1 mg/ml DPPC stock solution under nitrogen purging to avoid lipid contact with oxygen. The resuspended lipids were vortexed for 30 min to disperse the lipids in the buffer. The resulting solution was extruded at least 23 times at 50 °C through a polycarbonate membrane with a pore size of 0.1 μm to form unilamellar vesicles with a narrow size distribution.[22]

Hyaluronic acid (HA) stock solutions of 5 mg/ml were made by dissolving the HA in the buffer at 40 °C for 24 h with continuous stirring to ensure complete dissolution. The stock solution was diluted to a final concentration of 0.2 mg/ml of lipid and incubated with different concentrations of low and high MW HA for at least a day prior to any testing. HA compositions are listed in Table I.

Dynamic light scattering (DLS) measurements were conducted with a Nanostar Wizard (Wyatt Technologies) with a wavelength of 532 nm.

C. Small angle neutron scattering (SANS and USANS)

Small angle neutron scattering (SANS) measurements were performed on the extended q-range small-angle neutron scattering diffractometer (EQ-SANS) at the Spallation Neutron Source (SNS) at Oak Ridge National Laboratory (ORNL).[23,24] Three sample-to-detector distances (9, 4, and 2.5 m) in combination with wavelength bands defined by a minimum wavelength of 15, 10, and 2.5 Å, respectively, were used to cover the q-range of $0.003\ \text{Å}^{-1} < q < 0.3\ \text{Å}^{-1}$, where the magnitude of the scattering vector, q, is given by $q = (4\pi/\lambda)\sin(\theta)$. Here, λ is the wavelength of the neutron and 2θ is the scattering angle. Absolute scale intensities were calibrated with a porous silica standard sample.[25] Banjo cells (Hellma Inc., USA) of a 5 mm path length were used in all SANS measurements. All the measurements were conducted at 37 °C. Data reduction including corrections for

TABLE I. Hyaluronan concentrations added to 0.2 mg/ml DPPC vesicles in NaCl buffer (150 mM NaCl in D_2O or H_2O).

	Molecular weight (kDa)	Concentration (mg/ml)					
High MW HA	100–1000	0	0.1	0.33	0.5	1	1.5
Low MW HA	30–50	0	0.1	0.33	0.5	1	1.5

13 May 2024 08:52:55

© Author(s) 2023

detector sensitivity and background were performed using MANTIDPLOT software.[25,26] A spherical scattering length density (SLD) profile model built SASview V.5 was used to fit the SANS data to extract vesicle size and bilayer thickness.

Ultra-small-angle neutron scattering (USANS) measurements were performed on beamline-1A at the Spallation Neutron Source located at Oak Ridge Laboratory, Oak Ridge, TN.[24,27,28] Identical sample cells and conditions were used for EQ-SANS. The q-range covered in the USANS experiments was 10^{-5} Å$^{-1} < q < 5 \times 10^{-3}$ Å^{-1}.

D. Quartz crystal microbalance (QCM)

AT-cut quartz crystals (diameter = 25 mm) coated with gold (QSX 301, LOT Oriel Group, Germany) with a fundamental frequency of 4.95 MHz were used to study the surface-adsorption and structural transitions of the HA-DPPC mixtures in the NaCl buffer, prepared either with D_2O to compare to SANS experiments, or with millipore water, to study biomimetic conditions. Notably, the properties of the gold surface differ from those of the cartilage surface. For example, these gold surfaces have a higher wettability than cartilage, as the contact angle is ~50° for gold sensors versus 100° and 65° for healthy and diseased cartilage, respectively.[29,30] However, the reported wettability of cartilage was measured when exposed to air, that is, while drying, and hence, the contact angle is expected to be higher when immersed in SF. Furthermore, gold surfaces are smooth enough (RMS roughness ~ 1.3 nm) to enable us to image the adsorbed films in liquid by atomic force microscopy and distinguish the film morphology, which is impaired on rough surfaces.

Changes in frequency (Δf) and dissipation (ΔD) of the crystal resonator (Q-Sense, Sweden) were measured over different overtones (from n = 3 to n = 11), but the results presented here are at overtones of 5, 7, and 9, which are adequate for the thickness of the adsorbed films (tens of nanometers).[31–33] Gold sensors with a fundamental frequency of 4.95 MHz were cleaned by UV ozone for 10 min, immersed in a solution 5:1:1 mixture of MilliQ water: ammonia (25%): peroxide hydrogen (30%) at 75 °C for 5 min, rinsed with Milli-Q water, dried with N_2, and again treated with UV ozone for 10 min before use. Inlet and outlet tubing and the QCM chambers were rinsed with ultrapure water (GenPure UV, TKA GmbH, Niederelbert, Germany) before use. The fundamental frequencies were characterized in the NaCl buffer. The chamber is designed to provide a nonperturbing exchange of liquids over the quartz crystal by means of a pump. A flow rate of 20 μl/min was used, and the chamber temperature was maintained at 37 °C during all measurements.

E. Atomic force microscopy (AFM)

After adsorption, the QCM sensors with the adsorbed films were imaged by AFM (Nano Wizard, JPK Instruments, Germany) using the quantitative imaging (QI) mode with a sharp tip (HQ: CSC37, No Al, 0.3–0.8 N/m, Nanoandmore, USA). This method creates maps of height (or topography), adhesion, and surface stiffness. QI is the chosen mode of AFM imaging, since it eliminates the application of a lateral force, as it happens in contact mode imaging, and thereby, it minimizes artifacts due to drag or damage, which can happen to soft films. QI images ($10 \times 10\,\mu m^2$, $5 \times 5\,\mu m^2$, and $2 \times 2\,\mu m^2$) were postprocessed using the JPK software by subtracting a polynomial fit from the surface and replacing empty pixels by interpolation.

13 May 2024 08:52:55

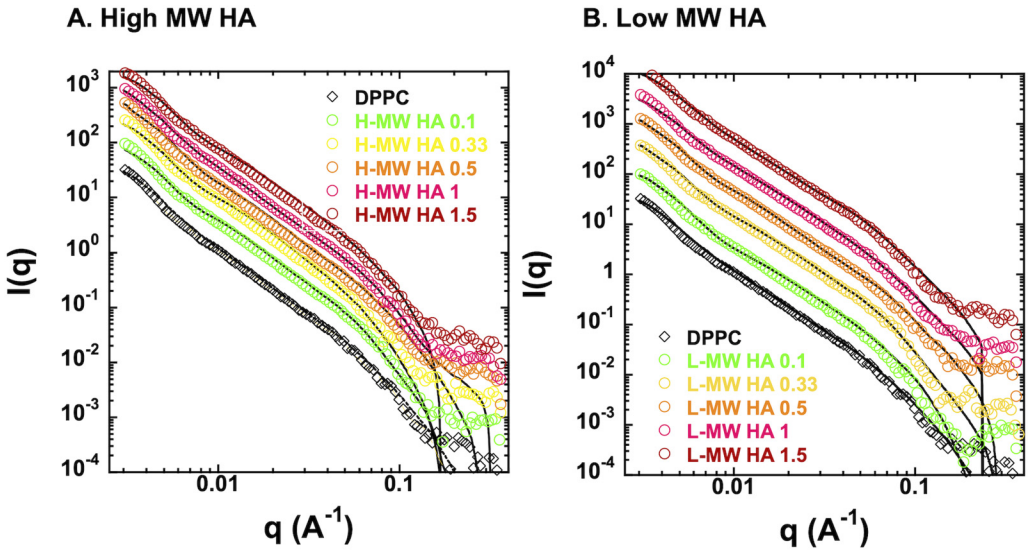

FIG. 1. SANS spectra of DPPC lipids with A, high MW and B, low MW HA at HA concentrations of 0.1, 0.33, 0.5, 1, and 1.5 mg/ml (see legend) in the NaCl buffer prepared with D_2O. The black diamonds correspond to the pure lipid solution. All solutions had a fixed concentration of 0.2 mg/ml DPPC and 150 mM NaCl. Scattering curves have been arbitrarily shifted on the y axis to improve clarity.

© Author(s) 2023

III. RESULTS

A. Change of vesicle size and bilayer thickness induced by low and high MW HA

Figure 1 shows the scattering curves obtained for DPPC vesicles, with the selected concentrations of low and high MW HA (Table I). The curves in Fig. 1 have been stacked on the y axis to enhance clarity. No scattering was measured for pure HA solutions. All scattering curves depict the characteristic form factor of spherical vesicles with a high polydispersity (PDI).[34] The absence of the characteristic lamellar peak at high q further confirms the unilamellarity of vesicles.[35] Additionally, a structure factor was not observed in the scattering data, which is expected for DPPC vesicles at low concentrations,[36] as well as HA solutions with added salt.[37] While no visibly distinct changes in the vesicle form factor are observed in Figs. 1(a) and 1(b), fits of the model [Eq. (1)] reveal subtle changes in the size and membrane thickness of vesicles as a function of the MW and concentration of HA.

Scattering intensities from unilamellar vesicles were modeled using a spherical core-shell form factor with smoothly varying interfacial functions; details of the model can be found in the supplementary material.[66] Since the vesicle concentration can be assumed to be well within the dilute concentration regime, scattering intensity can be written as

$$I(q) = nP(q)S(q) + I_{inc}, \tag{1}$$

where n is the number density of vesicles, I_{inc} is the incoherent background, $P(q)$ is the form factor of the vesicle of interest, and $S(q)$ is the structure factor describing the interaction between vesicles. Here, the structure factor can be approximated to be 1, since the concentration of vesicles is low enough.

The form factor of a spherical particle with a symmetric scattering length density (SLD) profile can be calculated by

$$P_{SLD}(q) = \frac{1}{V_{particle}}\left|4\pi\int_0^\infty \rho(r)\frac{\sin(qr)}{qr^2}r^2dr\right|^2, \tag{2}$$

where ρ(r) is the scattering length intensity (SLD) profile that can be defined as the linear sum of the core, two interfaces, and shell regions. The core represents the inner of the vesicle, where water is located. The shell represents the hydrophobic region of the bilayer, which has two boundaries (the two interfaces) and is defined by power-law functions. For the results discussed here, the PDI of the inner core was obtained to be 0.4 by initially using the PDI as one of the fitting parameters, along with all other structural parameters. In the next round of fittings, the PDI value was fixed at 0.4 to determine the values of the structural parameters; see all fitting parameters in Tables S1 and S2.[66] This approach led to better fits in the experimental data. The SLD of DPPC and D_2O were determined to be 0.2×10^{-6} Å^2, and 6.35×10^{-6} Å^2, respectively, based on their known molecular compositions and density.

Figure 2 summarizes the changes in vesicle radius and bilayer thickness as a function of HA concentration for the two investigated MWs, obtained by fitting Eqs. (1) and (2) to the scattering data. With no HA, the extruded DPPC vesicles have an average radius of ~36.8 ± 0.3 nm. The fits suggest that the vesicle radius decreases first with increasing concentration of high MW HA, until a minimum size is observed at a concentration of 1 mg/ml, with a radius of 34.7 ± 0.6 nm. The vesicle radius then increases with an increase in HA concentration to 1.5 mg/ml, yielding a maximum vesicle radius of 37.5 ± 1 nm. The addition of high MW HA induces a slight shrinkage of the lipid bilayer, in agreement with previous works.[17,18] Here, the bilayer thickness decreases from

13 May 2024 08:52:55

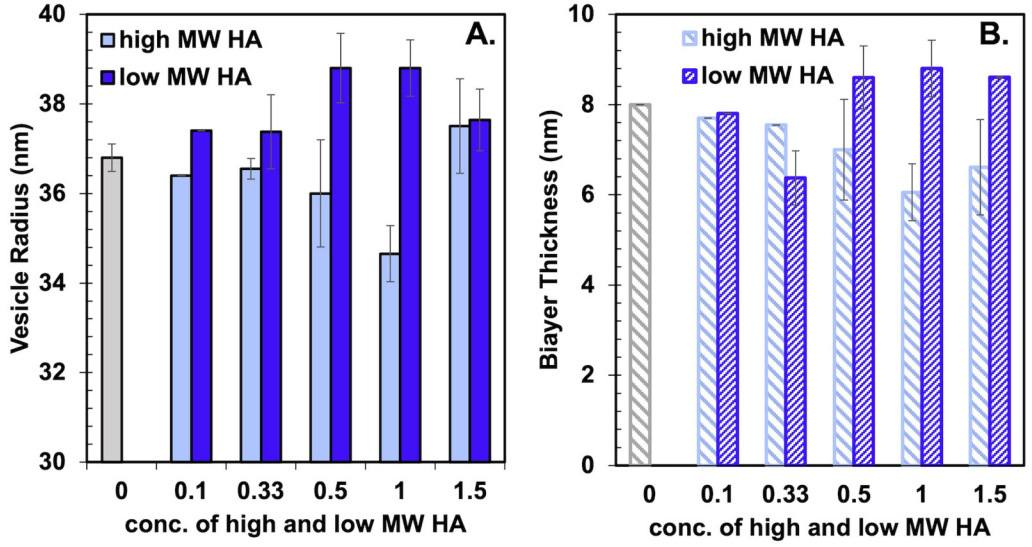

FIG. 2. Results for A, radius and B, bilayer thickness of HA-DPPC vesicles obtained from fitting Eqs. (1) and (2) to the SANS spectra. The dashed arrows serve as a guide to the eye. The results at 0 mg/ml HA correspond to pure DPPC vesicles.

© Author(s) 2023

~79.9 Å to ~66.1 Å, as the concentration of high MW HA increases from 0 to 1.5 mg/ml. The results with low MW HA are quite different. First, the radius of vesicles increases with concentration, with the largest radius measured at 0.5 and 1 mg/ml (~38.8 nm), and then it decreases to ~37 nm with a further increase in concentration to 1.5 mg/ml, yielding opposite changes compared to high MW HA. The bilayer thickness with low MW HA decreases down to 63 Å with a concentration up to 0.33 mg/ml, i.e., more notably than with high MW HA, and it increases to ~86 Å with a further increase in concentration. Interestingly, the calculated bilayer thickness at a concentration of 0.5 mg/ml low MW HA and above is, thus, larger than that of the reference DPPC vesicles. These findings together show that the structural response due to the interaction with HA is clearly dependent on the molecular weight (or the length) of HA.

B. High MW HA leads to the aggregation of vesicles

Size measurements of lipid-HA mixtures using DLS are summarized in Fig. 3 as a function of HA MW and its concentration; the DLS results for pure HA solutions are displayed in Fig. S3,[66] for reference. The radius of pure lipid vesicles, i.e., with no added HA, was measured to be ~38.4 ± 2.3 nm, with a PDI of 0.16. Figure 3(a) shows the average values of the three detected peaks; the error bars show the standard deviation and the size of the bubble gives the relative intensity of each peak. The discussion is focused on the peak with the highest intensity [peak 2 in Fig. 3(a) and peak 3 in Fig. 3(b); see details in the caption].

The addition of low MW HA led to a small increase in the radius of vesicles; that is, 45.9 ± 2.7 nm, 42.1 ± 3.5 nm, 46.7 ± 3.4 nm, 44.7 ± 5.5 nm, and 46.6 ± 3.8 nm, for 0.1, 0.33, 0.5, 1, and 1.5 mg/ml of low MW HA, respectively. The PDI also increased from 0.16 for the vesicles to 0.32, 0.26, 0.30, 0.25, and 0.31, respectively (see labels). It should be noted that the equilibrium size of the low MW HA in the reference stock solution in the NaCl buffer is ~9 nm,[38] and hence, notably smaller than the size measured by DLS.

The addition of high MW HA to the vesicle solution leads to a more significant increase in the size of the assembled structures [peak 3 in Fig. 3(b)]. The average radius of peak 3 increases in direct proportion to the HA concentration. That is, the radius of the HA-lipid structures is 50.1 ± 4.8, 70.5 ± 8.8, 128.3 ± 30.3, 132.3 ± 14.4, and 182.5 ± 34.4 nm for HA concentrations of 0.1, 0.33, 0.5, 1, and 1.5 mg/ml, respectively. The PDI depends on high MW HA concentration and is very high (0.41, 0.34, 0.32, 0.33, and 0.35 for 0.1, 0.33, 0.5, 1, and 1.5 mg/mL, respectively). The reference DLS measurements for high MW HA in the absence of lipid show a wide size distribution with two broad peaks, one with an average around 30–40 nm, and a second one pointing at much larger structures with an average ranging from 350 to 550 nm, for the investigated concentrations; see Fig. S3.[66] Hence, the size distribution for the high MW HA-lipid mixtures is much narrower, with one distinct and prominent peak, whose average radius increases proportionally with the HA concentration. Peak 2 in Fig. 3(b) is most likely due to high MW HA chains dispersed in the solution, while peak 1 (<2 nm) is most likely a measurement artifact. Note that these bubbles are very small indicating that their contribution is not significant.

The DLS results for high MW HA, along with the inferred vesicle and bilayer structure from SANS, suggest that the radii detected by DLS (peak 3) can be a representative of aggregated vesicles via high MW HA. Indeed, USANS measurements also show the formation of a traversing network of HA with vesicles in solution at 1.5 mg/ml (Fig. S2).[66] This is expected as the polymer

13 May 2024 08:52:55

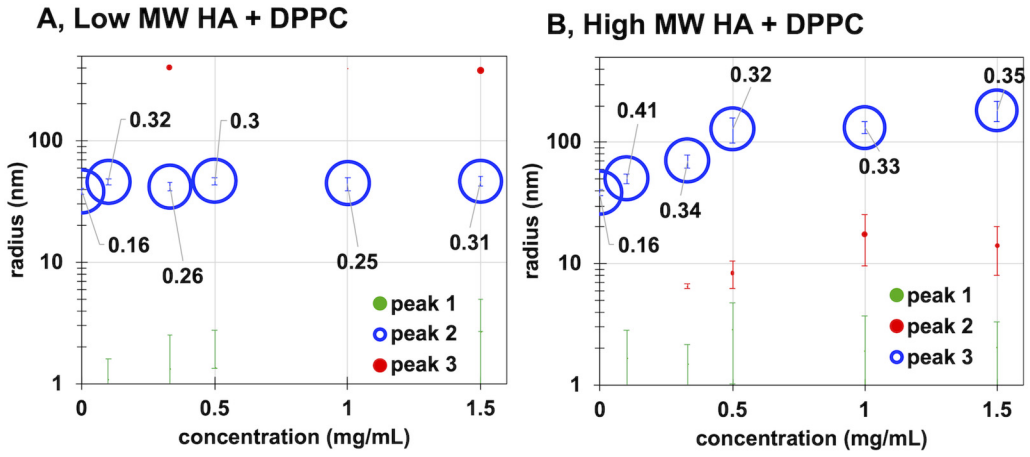

FIG. 3. Size (radius) of lipid-HA mixtures measured by DLS as a function of the HA concentration for the A, low and B, high MW HA. The DPPC concentration was fixed at 0.2 mg/ml. Both systems exhibit a multimodal size distribution. The plots are bubble diagrams that show the average radius of each peak, the error bars show the standard deviation, and the size of the bubble represents the relative intensity of each peak. Both HA-lipid mixtures exhibit one prominent peak (in blue, peak 2 for low MW HA and peak 3 for high MW HA. The label shows the polydispersity index of the most prominent peak. Peak 1 is likely an artifact of the measurement. 1000 kDa polymer may have a radius of gyration of around 8 nm (Ref. 39), and hence, peak 2 (red) in B, suggests the assembly of free HA chains. Ten measurements were conducted per composition and the bubble diagrams show the average of these 10 measurements. Green bubbles are so small that cannot be seen.

© Author(s) 2023

solution changes from a dilute to a semidilute regime[40] and it points to a critical change of behavior at 1.5 mg/ml high MW HA, which needs further investigation.

The intricate changes of the vesicle size for high MW HA revealed by SANS differ significantly from the DLS results [cf. Figs. 2 and 3(b)]. In DLS, the vesicle size consistently increases with the addition of HA. Instead of sharp multimodal size distributions, DLS shows broad peaks with large polydispersity, supporting the formation of HA-lipid vesicles and aggregates of varying sizes, where the increasing size reflects the increasing content of HA. In addition to this, we cannot exclude the presence of free HA polymers in the solution. SANS, however, only detects comparatively smaller single vesicles. This discrepancy is attributed to the different measuring principles, where DLS measures the average aggregate size, whereas SANS probes the contrast between individual vesicles and bulk. Importantly, only slight changes of the individual vesicle and bilayer size were observed per SANS analysis, indicating that even in the HA/lipid aggregates implied by DLS, the individual vesicles greatly maintain their initial structure. We also note that the DLS radii of the low MW HA-lipid structures are larger than the values determined by SANS [cf. Figs. 2 and 3(a)]. We associate this with the fact that SANS is not sensitive to the protruding HA chains from vesicles; see the proposed assembly in Sec. IV.

C. Amorphous layer resulting from the self-assembly of high MW HA-DPPC on gold sensors

Figure 4 shows representative QCM-D measurements of DPPC with 0, 0.1, 0.33, 0.5, 1, and 1.5 mg/ml high MW HA. This plot also shows the QI-mode AFM images of the QCM gold sensors after adsorption, specifically, the topography, surface stiffness, and adhesion maps. Multiple images (at least 5) on each sensor were taken to confirm reproducibility. For reference, Fig. S4 in the supplementary material[66] shows the QI images of the bare gold sensors, with a roughness of ∼1.29 nm RMS, an average surface stiffness of ∼52 nN/μm, and an average adhesion of ∼7.3 nN to a sharp silicon tip. The average stiffness and adhesion values were determined by fitting a gaussian distribution to the histograms extracted from the respective QI images. QCM and AFM studies were performed in the NaCl buffer with H_2O to mimic biological conditions, but the results with the samples prepared in D_2O led to similar conclusions, as described later.

Figure 4(a) shows the results for DPPC vesicles. The initial frequency decrease with a concurrent large increase of dissipation indicates fast vesicle adsorption. Adsorption rapidly slows down and equilibrium is not achieved after ∼1h. This is inconsistent with the classical fingerprint of vesicle rupture, where the frequency would display a sharp decrease followed by a rapid increase in frequency during adsorption, equilibrating at $\Delta f \sim 25$ Hz and $\Delta D \sim 1–2 \times 10^{-6}$ for a lipid bilayer on a QCM sensor of the characteristics used here.[41] Thus, while there may be some rupture, the vast majority of vesicles remain intact on the surface. While rinsing with buffer (see gray arrow), dissipation decreases to $\Delta D_7 \sim 38 \times 10^{-6}$ and frequency increases to $\Delta f_7 \sim -164$ Hz, which reflects that some adsorbed vesicles may either desorb or rupture, but the majority of them stay intact on the surface. Figure S5 in the supplementary material[66] shows a plot of dissipation versus frequency (D−f) for DPPC vesicles. The fact that the D−f plot essentially follows the same path after rinsing tends to suggest a reversible process, i.e., the reversibly bound material from the latter part of the adsorption phase is rinsed off.

Stiffness maps corresponding to the adsorbed DPPC vesicles show very soft and deformable domains occupying 50% of the total surface, with high adhesion to the tip compared to the surrounding surface. The surface-immobilized vesicles exhibit a wide height distribution and different extents of lateral spread, which leads to a large RMS roughness (average∼19.2 nm). Most of the domains exhibit a height of ∼80 nm and a width of ∼120–150 nm or 35 nm height with a larger lateral spread (see cross sections in Fig. S6).[66] Note that imaging these domains can also induce a deformation due to the applied force by the tip (0.7 nN). The images also show flat domains with a height of ∼14 nm, which may be associated with the partial rupture of DPPC vesicles. Because this height is much larger (around a factor of two) than the thickness of a bilayer measured by SANS, it is more likely to be associated with the assembly of two bilayers on the surface. These AFM results also support that most of the DPPC vesicles do not rupture on the surface.

At the concentration of 0.1 mg/ml high MW HA [Fig. 4(b)], there is an initial fast drop in frequency, yet slower than for DPPC vesicles [cf. Fig. 4(a)], which indicates that the affinity of HA-DPPC to the surface is decreased in the presence of HA at a small concentration. This is not surprising considering the expected steric and electrostatic repulsion for high MW (negatively charged) HA. This is followed by a step, during which the dissipation increases slowly from $\Delta D_7 \sim 14$ to $\sim 20 \times 10^{-6}$ and the frequency decreases from $\Delta f_7 \sim -105$ to ~ -123 Hz in ∼1.2h. The slow frequency change as a function of time has been previously reported to be indicative of a reorganization of the adsorbed layer,[42] which could be happening here, as well. There are no clear signs of vesicle rupture in QCM experiments. Equilibrium is not achieved even after ∼2h (Fig. S7).[66] AFM shows the presence of a soft film (average stiffness ∼4.3 nN/μm) with a smaller RMS roughness of 4.6 nm, and a much smaller average adhesion (∼37 pN) compared to DPPC on gold surfaces, consistent with the full coverage of the surface with a soft film. The cross sections (Fig. S8)[66] reveal mainly flat domains with a height of ∼12 nm and a width of ∼100–150 nm [Fig. S8(A)], which might result from the assembly of one or two bilayers on the surface. At some spots, adhesion is much higher than the average value [see white spots in Fig. S8(B)], while the surface stiffness is much smaller than the surrounding region, which is attributed to the presence of some intact vesicles. The maximum film thickness at these locations is ∼35 nm, i.e., similar to the vesicle radius as determined by SANS (∼37 nm), which indicates that they undergo significant deformation upon interaction with the surface and the tip.

The initial adsorption of HA-DPPC vesicles becomes faster upon an increase in concentration to 0.33 and 0.5 mg/ml high MW HA, as shown by the steeper decrease in frequency compared to 0.1 mg/ml, perhaps because the diffusion rate to the surface increases with concentration and/or because a higher near-surface concentration enhances the probability of adsorption. Also here, a plateau is not achieved during the first hour of adsorption. The frequency ($\Delta f_7 = -108$ and -103 Hz for 0.33 and 0.5 mg/ml, respectively) and dissipation ($\Delta D_7 = 13 \times 10^{-6}$ and 21×10^{-6} (−),

13 May 2024 08:52:55

© Author(s) 2023

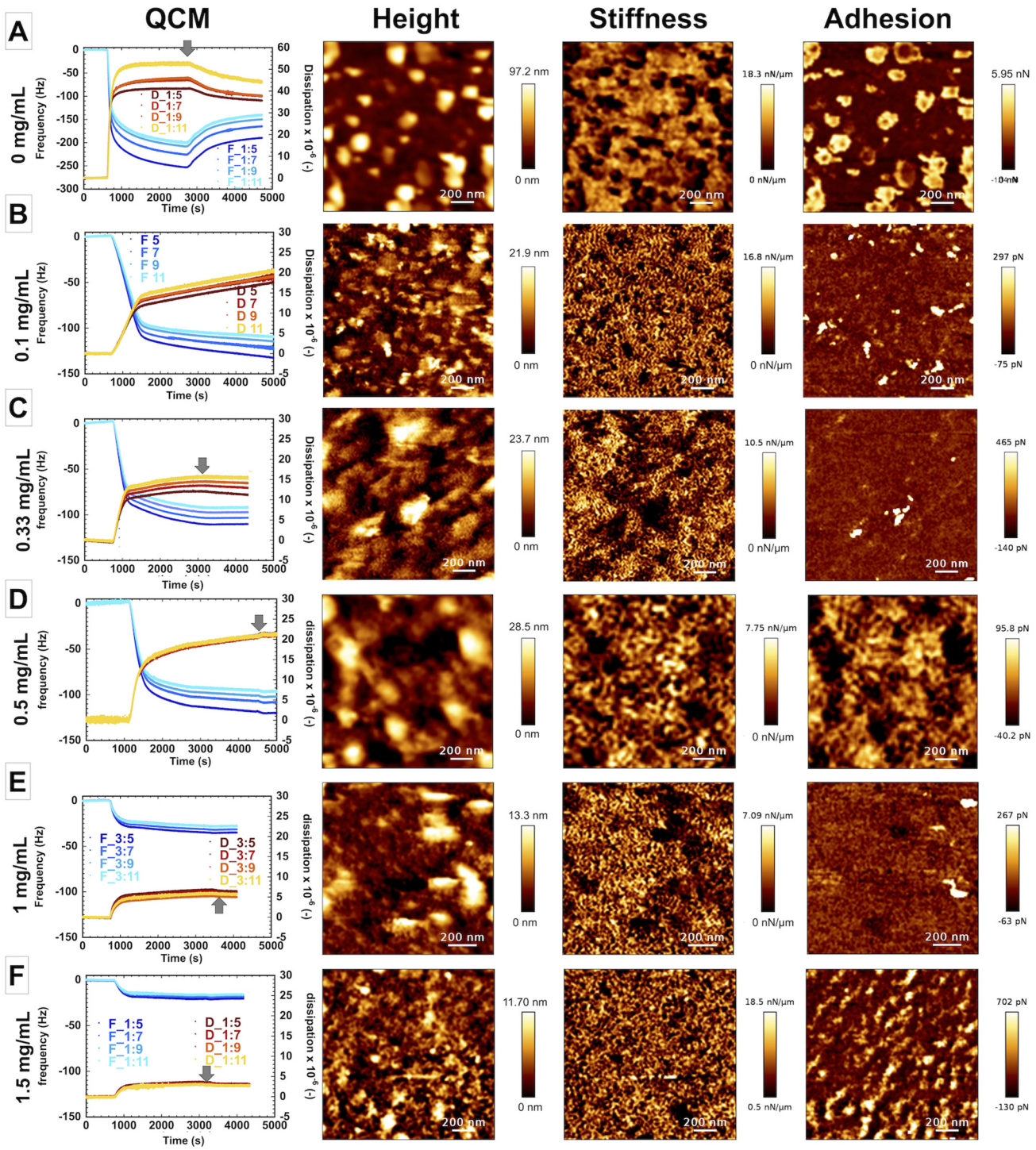

FIG. 4. Frequency and dissipation (first column) as a function of time for the adsorption of high MW HA-lipid vesicle mixtures on gold sensors, height map (second column), surface stiffness (third column), and adhesion map (fourth column). The HA concentration is (a) 0, (b) 0.1 mg/ml, (c) 0.33 mg/ml, (d) 0.5 mg/ml, (e) 1 mg/ml, and (f) 1.5 mg/ml, and the DPPC concentration is 0.2 mg/ml DPPC, all in the NaCl buffer with water. The legend in QCM plots in (b) and (c) is the same as in (a) and (e)-(f). Four overtones are shown (3, 5, 7, and 9). The gray arrow in each plot indicates the rinsing step with a buffer. Negative adhesion means repulsive interaction.

13 May 2024 08:52:55

© Author(s) 2023

respectively) after rinsing with buffer are similar to that at 0.1 mg/ml, but the film morphology differs significantly.

Figures 4(c) and 4(d) show films with much larger domains, larger average thickness as, well as greater RMS roughness (7.7 and 7 nm, respectively) at 0.33 and 0.5 mg/ml compared to 0.1 mg/ml. The average surface stiffness (2.9 and 2.8 nN/μm, respectively) and average adhesion (47 and 28.5 pN, respectively) remain small, consistent with the full coverage of the surface with a film. At 0.33 mg/ml, there are many flat domains with a height of ~15 nm and a width of several 100s nanometers [Fig. S8(D)],[66] but also a few domains resembling deformed vesicles [Fig. S8(C)]. A further increase of HA concentration to 0.5 mg/ml yields both types of domains but are now similarly distributed [Figs. S8(E) and S8(F)]. The cross sections show vesicles with a height of ~30–50 nm and a width of 150–200 nm at HA concentrations at 0.33 and 0.5 mg/ml. They are highly deformable and often unstable; so they rupture during imaging, especially with an increase in concentration. Interestingly, at a concentration of 0.33 mg/ml, they correlate with high adhesion, whereas at 0.5 mg/ml, they correspond to low-adhesive domains (Fig. S9).[66] This might point toward the compositional change of these regions with the increase of HA content, which reduces the interaction with the (negatively) charged tip. (However, we cannot completely exclude the possibility that the lipids released during vesicle rupture coated the tip, which would also influence the interaction with the surface film.) QCM and AFM experiments were also performed with only high MW HA (in the absence of lipids) for reference. In this case, the adsorption of HA is poor at concentrations ≤0.5 mg/ml [Figs. S10(A) and S10(B)],[66] [$\Delta f_7 < 8$ Hz, $\Delta D_7 < 1 \times 10^{-6}$ (−)], and hence, it significantly differs from the HA-lipid films that form in the same concentration range.

A further increase in HA concentration leads to significantly different results for HA-lipid vesicles. At 1 mg/ml, the frequency plateaus are at $\Delta f_7 \sim -31$ Hz and $\Delta D_7 \sim 6.1 \times 10^{-6}$ (−), which indicates the reduction of the adsorbed mass of HA-DPPC on the gold surface [Fig. 4(e)]. Consistent with QCM results, QI images at 1 mg/ml high MW HA show a significant reduction of the film thickness and RMS roughness (4.5 nm), while the average adhesion and surface stiffness remain small (average values ~85 pN and 2 nN/μm), supporting the full coverage of the surface with a soft film. The cross sections in Figs. S8(G) and S8(H) show the presence of deformed vesicles on the surface, with heights of ~40 nm and widths of 200 nm or more, but less crowded on the surface than at lower concentrations. Interestingly, the adsorption of high MW HA at 1 mg/ml (reference, no lipid) is promoted compared to lower HA concentrations [$\Delta f_7 \sim -10$ Hz and $\Delta D_7 \sim 2 \times 10^{-6}$ (−)], the adsorption rate is faster [Fig. S10(C)], and leads to a homogeneous thin film.

Figure 4(f) shows that a further increase of the HA concentration to 1.5 mg/ml leads to a smaller decrease (increase) of frequency (dissipation) in QCM experiments [$\Delta f_7 \sim -17$ Hz and $\Delta D_7 \sim 3.2 \times 10^{-6}$ (−)], which indicates that the adsorption of lipid-HA vesicles is further hindered compared to 1 mg/ml. This coincides with a decrease of the average film thickness and the RMS roughness (~3.3 nm) and, notably, a slight increase in the average adhesion and surface stiffness (124 pN and 6 nN/μm, respectively), which can be justified by the adsorption of a thinner film on the surface. Furthermore, the regions with high adhesion correspond here to high stiffness and low height, consistent with the characteristics of the gold substrate, and hence, with the partial coverage of the surface. The morphology of the films is also clearly different from that at smaller concentrations (0.33–1 mg/ml), as now, a finer network can be observed. The domains are flat and exhibit a height of ~50 nm, but there are also a few domains with a smaller height of ~14 nm [Figs. S8(I) and S8(J)].

Figure 5(a) summarizes the changes in frequency and dissipation for the investigated concentrations of high MW HA. The results are close to a stepwise reverse isotherm, i.e., an increase in concentration leads to a decrease in adsorbed mass (less negative Δf), with a step at around 0.5 mg/ml. This isotherm type suggests the action of competitive adsorption. Figure 5(b) displays the rate of frequency change during the initial adsorption step and also reveals nonmonotonic trends, suggesting the presence of at least three, if not more, mechanisms governing the adsorption of HA-lipid mixtures. Based

13 May 2024 08:52:55

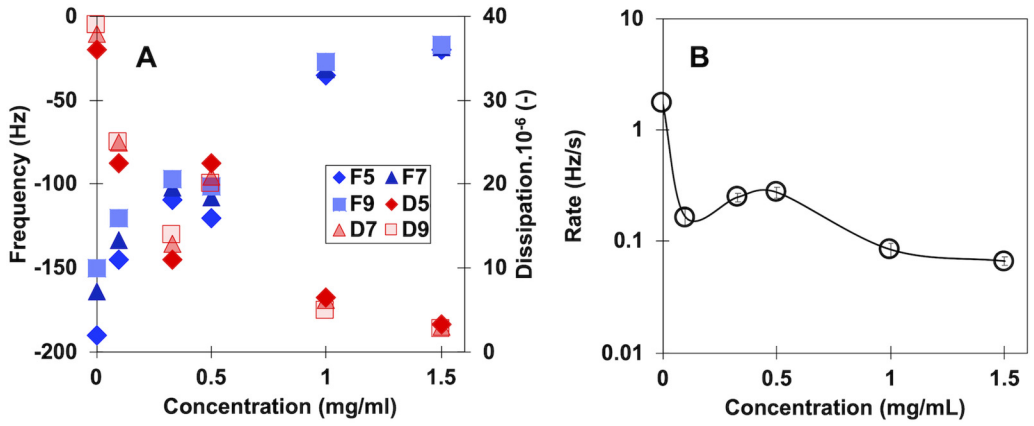

FIG. 5. (a) Overall change of frequency (left axis) and dissipation (right axis) vs the concentration of high MW HA for the adsorption of HA-lipids after rinsing with buffer. (b) Change in frequency over time during the initial adsorption of HA-lipids as a function of high MW HA concentration.

© Author(s) 2023

on the DLS results, it is most likely that there is competition between all the present structures (vesicles and their aggregates as well as free HA), and at the very highest concentration, free HA is able to dominate adsorption, leading to the observed final decrease in the adsorption rate and low adsorbed mass.

Samples prepared in NaCl buffer with deuterated water were also investigated by QCM and AFM at HA concentrations of 0, 0.1, 0.33, and 1.5 mg/ml to confirm that the film structure is not affected by the solvent used in the sample preparation or during the rinsing step; representative results are shown in Fig. S11.[66] The adsorption behavior was reproduced in the buffer with deuterated water, except at the concentration of 0.1 mg/ml. In this case, most of the adsorbate exhibits heights of 30–50 nm and widths between 100 and 200 nm, but there is also a significant aggregation of vesiclelike structures on several spots with much greater heights (see Figs. S12 and S13).[66] The adsorption behavior of these large aggregates is not represented by the QCM results in Fig. S11(B), which suggests that aggregation could happen after adsorption due to vesicle motion on the surface. In contrast, Fig. 4(b) shows the formation of a continuous but rough film on the surface of the samples prepared in a buffer with water. The origin of this difference has not been deciphered yet, and hence, we consider that both scenarios are possible at low concentrations of high MW HA.

D. Hindered adsorption of complexes of DPPC and low MW HA

QCM measurements show a very small amount of low MW HA-DPPC mixtures on the gold surface; $\Delta f \sim 2-5$ Hz and $\Delta D < 3 \times 10^{-6}$ (−). This can be explained by either the low adsorption of complexes due to their low affinity to gold or by their sedimentation. In either case, a weaker interaction of vesicles with the gold surface indicates that the adsorption of HA-lipid vesicles significantly depends on the MW of HA. Representative QI images are shown in Fig. 6 along with the QCM results at the concentration of 0.33 mg/ml, but the results at other concentrations in the range of 0.1–1.5 mg/ml are qualitatively similar (not shown). Importantly, the adhesion maps show regions of low and high adhesion within the structure of the adsorbed vesicles, thereby suggesting the presence of gradients in composition (e.g., HA rich and poor regions).

IV. DISCUSSION

The influence of the MW of HA on the structure of HA-lipid vesicles is remarkable. With low MW HA, their size is larger than that of pure DPPC vesicles [Fig. 2(a)]. In addition, the fits to SANS results reveal that the lipid bilayer exhibits a compression at 0.33 mg/ml compared to pure lipid vesicles, while above this concentration, the bilayer thickness increases. The effect of HA on vesicle size and bilayer thickness can be justified by the distribution of low MW HA either adsorbed onto or intercalated into the DPPC bilayer to maximize its hydrophobic contacts. Indeed, a key feature of the twofold helix structure of HA is its extensive hydrophobic patch.[43] Multiple studies have emphasized the dominant mechanism of the adsorption of HA on DPPC membranes to be also of a hydrophobic nature[44–46] and that this interaction is highly dependent on the morphology of the HA molecule, i.e., on the number of hydrophobic and hydrogen bonding sites accessible to the DPPC membrane.[47] The intercalation of the hydrophobic motifs of HA into the lipid bilayer has been reported by Zander *et al.*[48] MD simulations have also revealed that low MW HA can accumulate within the condensed DPPC domains.[49] Simulations have also shown that the number of hydrophobic contacts between a short HA molecule and the DPPC membrane is far greater than the hydrogen bonds that can form between them, as the process of forming a hydrogen bond requires breaking a DPPC-water hydrogen bond first.[50]

Figure 7(a) shows schematics of the proposed intercalation of low MW HA into the bilayer. The incorporation of low MW HA into the bilayer could explain the observed expansion above 0.33 mg/ml. On the other hand, DPPC is zwitterionic, while HA is negatively charged in the solution. At high sodium concentrations, like in this study, electrostatic repulsion between the phosphate headgroup of the lipid and the negatively charged HA is screened,[51,52] which reduces the electrostatic repulsion, and thereby, favors the configuration displayed in Fig. 7(b), left. Such a configuration would justify the compression of the bilayer. The distribution of low MW HA in the membrane is unknown, but adhesion maps suggest that there are compositional gradients.

A very different bilayer structure is suggested for high MW HA-DPPC, where a significant decrease in vesicle size and bilayer thickness is observed at concentrations <1.5 mg/ml. This suggests that the vesicles cannot accommodate high MW HA within the bilayer. It is possible that the hydrophobic interaction between HA and DPPC vesicles is not thermodynamically favorable under the

13 May 2024 08:52:55

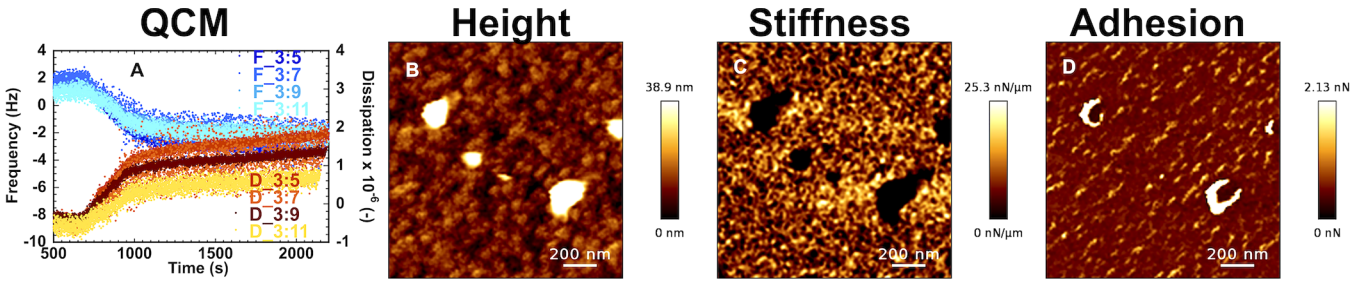

FIG. 6. Frequency and dissipation as a function of time during the adsorption of low MW HA-DPPC mixtures at 0.33 mg/ml in NaCl buffer on gold sensors (first column), height map (second column), surface stiffness (third column), and adhesion map (fourth column). Four overtones are shown (5, 7, 9, and 11).

© Author(s) 2023

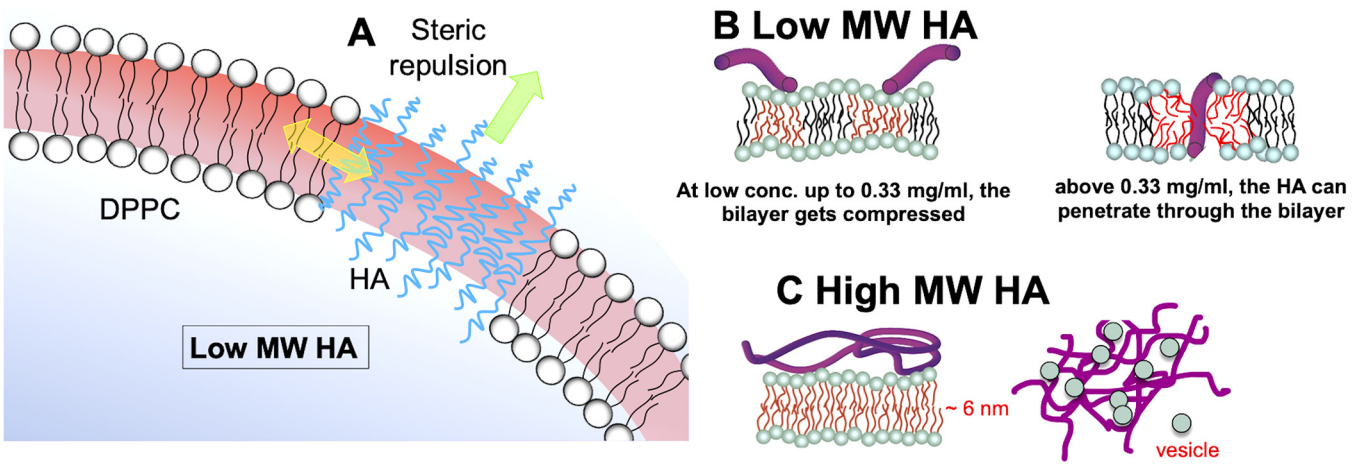

FIG. 7. Effects of HA concentration and MW on the interaction between HA and DPPC vesicles and the resulting configuration. Conceptual picture for A-B, low MW HA below and above 0.33 mg/mL, and C, for high MW HA.

selected experimental conditions, due to the much larger entropic cost of high MW HA to self-assemble in the membrane. In other words, the conformational change required for HA to intercalate into the bilayer is prohibited for high MW HA—while it is possible for low MW HA. Figure 7(c) shows potential configurations of high MW HA. High MW HA could assemble on the bilayer. Based on the DLS results, HA could also interact with DPPC located in different vesicles leading to the aggregation of several vesicles. A larger structure comprising of a HA network with embedded vesicles could justify the compression of vesicles leading to fluid exudation.[53,54] With increasing HA concentration, the probability of the interaction between HA and DPPC should increase, which could lead to more defective vesicles, justifying the reduction of their size.[55] This configuration is also consistent with the vesicle aggregation observed by DLS—and more so, with an increase in concentration. Interestingly, QCM experiments with high MW HA-DPPC mixtures often show a slow and steady change in Δf and ΔD so that equilibrium is not achieved over hours (Fig. 4). This could reflect the change of the conformation of HA and lipids within the adsorbed film on the sensor. Such structural changes of the film would be consistent with the weak interaction between high MW HA and lipids. Indeed, the absence of interactions between DPPC vesicles and high MW HA has been reported before.[17,56] We also note that the reduction of the bilayer thickness is in contradiction to previous studies.[48,57,58]

The fact that the bilayer compression and expansion with low MW HA are more significant than the changes induced by high MW HA supports that low MW HA interacts more strongly with lipid vesicles, in agreement with previous studies.[18,59] One reason might be related to the fact that at the same mass concentration in solution, the number of HA chains with low MW is higher (2–30 times), which might promote the interaction with lipids. The results at 1.5 mg/ml high MW HA—increase in vesicle size and bilayer thickness after achieving a minimum at 1 mg/mL, concurrent with aggregation—are intriguing and call for additional investigations in the regime of high concentrations.

A. Biotribological implications

The HA-DPPC films that form at 0.1–0.5 mg/ml high MW HA exhibit a similar structure to the amorphous layer previously reported by Crockett *et al.* for DPPC and HA.[60] The high roughness (from AFM) and dissipation (QCM) of the surface films are not consistent with a well-ordered bilayer structure, but instead with the formation of a highly dissipative, soft, disordered lipid-HA film. The addition of high MW HA preserves the affinity of vesicles to the surface but enables the reorganization of lipids and HA upon interaction with the surface, and thereby, the formation of an amorphous film. The increasing size of vesicles detected by DLS (50.1 ± 4.8, 70.5 ± 8.8, 128.3 ± 30.3 for HA concentrations of 0.1, 0.33, and 0.5 mg/ml, respectively) points toward the entanglement of vesicles via HA, which should favor the formation of a continuous thick film that fully covers the surface, if adsorption happens. Based on the morphologies revealed by AFM, it is difficult to determine how many vesicles rupture or remain intact in this amorphous layer.

It is also evident that an excess of high MW HA (~1 mg/ml) reduces the adsorption of HA-DPPC on the gold surface and leads to a drop in film thickness and a change in film morphology. This could be related to the negative charge of HA, electrostatically repelled from the surface. However, considering the high ionic strength of the buffer, it seems more reasonable to associate the reduced adsorption with an enhanced steric repulsion with concentration. It is also interesting that SANS shows a change of vesicle structure (minimum in size and bilayer thickness) at 1.5 mg/ml, concurrent with the different morphology of the surface film. As described earlier, this regime of high concentration requires further investigation.

We speculate that the formation of an amorphous layer is key to providing hydration and efficient boundary lubrication to a healthy articular joint. At concentrations up to 0.5 mg/ml, the films are soft and nonadhesive. These thick films also help to maintain some vesicles intact, i.e., to prevent, at least partially, their rupture. Highly dissipative and nonadhesive amorphous layers have been

13 May 2024 08:52:55

© Author(s) 2023

hypothesized to maintain low friction at the cartilage surface. It is to be noted that the role of intact vesicles at the articular interface has been previously explored by Sorkin *et al.*[61] This work correlated the lower friction coefficient with the presence of liposomes at the interface. Furthermore, previous reports on the effect of HA on the surface adsorbed layers of phospholipids have demonstrated an increase in mechanical robustness,[48] which is expected to provide a higher load-bearing capacity and wear resistance, and thereby, more efficient boundary lubrication.

With an increase in high MW HA concentration, the film thickness decreases, and its morphology changes, as more HA adsorbs and more vesicles rupture. While this behavior is characteristic for the formation of the HA-lipid film on gold, we can expect that competitive adsorption between HA, lipids, and other components in the SF, will also happen on the cartilage surface, and the lubricious boundary layer will form at an optimal HA concentration or concentration range. The optimal concentration could differ from the one reported here for a simplified system, lipids and HA on gold. It is also worth noting that the MW of HA in healthy joints can be larger than 1 MDa (Table I). Increasing the MW of HA above the range investigated here might induce more vesicle aggregation, and increased adsorption of HA-lipid complexes, and thereby, thicker boundary films. This is a hypothesis that needs to be proven, though.

The combination of QCM and AFM demonstrates that low MW HA significantly hinders vesicle adsorption, which could also happen on other biological interfaces. In arthritic cartilage, high MW HA can still be present in the SF but at a much lower content than in healthy cartilage.[62] If a mixture of low and high MW HA is present, it is reasonable to expect competitive adsorption, and hence, low MW HA impairs the formation of the boundary layer, and it even dominates the surface adsorption at a very low content of high MW HA. If vesicles with low MW HA adsorb, the insertion of HA into the lipid membranes, however, warrants that low MW HA would contribute to reduced friction during articulation via boundary lubrication. However, the lack or loss of the amorphous layer is expected to negatively impact the mechanical integrity and longevity of the boundary layer. We speculate that this may contribute to the increased wear of the cartilage that has been reported in joints diseased with OA.[63,64] Studies on HA itself and HA-lipid complexes do not entirely support HA's role in providing high lubricity to the cartilage's articular surface.[65] Our results for low MW HA also indicate that more focused studies combining MD simulations and neutron reflectometry can help to shed light on the intricate interactions between HA and DPPC vesicles and their connection to friction and wear.

V. CONCLUSIONS

We have investigated the structural changes of HA-DPPC mixtures as a function of HA concentration with high and low MW, to simulate the physiologically relevant conditions that exist in healthy and diseased joints, respectively. SANS and DLS were used to determine the structure of HA-lipid vesicles in bulk solution, while a combination of quartz crystal microbalance and atomic force microscopy was used to study their assembly on a gold surface and the morphology of the films. Our results have shown the influence of the MW and HA concentration on the size and bilayer thickness of HA-lipid vesicles. Furthermore, SANS results are consistent with the intercalation of low MW into the bilayer, which seems to be prohibited for high MW HA. High MW HA promotes the aggregation of vesicles, and more so, with an increase in concentration. Upon assembly of HA-DPPC on gold surfaces, the thickness and morphology of the surface-adsorbed films still depend on MW and the concentration of HA. High MW HA forms thick amorphous layers on the gold surface at concentrations smaller than 1 mg/ml, which are expected to provide a higher load-bearing capacity and wear resistance, and thereby, more efficient boundary lubrication. Higher concentrations of high MW HA also reduce surface-adsorption of vesicles, which suggests that there is an optimum concentration for the formation of boundary films based on the structure of HA-DPPC vesicles in the bulk. Low MW HA greatly hinders vesicle adsorption and the formation of a thick film. We propose that this may contribute to the increased wear of the cartilage that has been reported in joints diseased with OA, where low MW HA is more abundant.

ACKNOWLEDGMENTS

This article is based on work supported by the National Science Foundation under Grant Nos. CMMI 17-61696, CMMI 20-35122, and CMMI 21-21681. The research was carried out in part in the Materials Research Laboratory Central Research Facilities, University of Illinois. This research used resources at the Spallation Neutron Source, a DOE Office of Science User Facility operated by the Oak Ridge National Laboratory.

13 May 2024 08:52:55

AUTHOR DECLARATIONS

Conflict of Interest

The authors have no conflicts to disclose.

Ethics Approval

Ethics approval is not required.

Author Contributions

Kangdi Sun: Conceptualization (equal); Formal analysis (lead); Funding acquisition (equal); Investigation (lead); Methodology (lead); Supervision (equal); Visualization (equal); Writing – original draft (lead); Writing – review & editing (supporting). **Tooba Shoaib:** Conceptualization (lead); Formal analysis (equal); Investigation (lead); Methodology (lead); Supervision (equal); Visualization (equal); Writing – original draft (lead); Writing – review & editing (supporting). **Mark W. Rutland:** Conceptualization (supporting); Formal analysis (equal); Investigation (lead); Methodology (equal); Supervision (equal); Visualization (equal); Writing – original draft (lead); Writing – review & editing (equal). **Joesph Beller:** Investigation (equal); Methodology (supporting). **Changwoo Do:** Conceptualization (equal); Methodology (equal); Supervision (equal); Visualization (supporting); Writing – review & editing (equal). **Rosa M. Espinosa-Marzal:** Conceptualization (equal); Formal analysis (equal); Funding acquisition (equal); Methodology (supporting);

© Author(s) 2023

Supervision (equal); Visualization (equal); Writing – original draft (lead); Writing – review & editing (lead).

DATA AVAILABILITY

The data that support the findings of this study are available within the article and its supplementary material.

REFERENCES

[1]A. J. Sophia Fox, A. Bedi, and S. A. Rodeo, Sports Health: Multidiscipl. Approach **1**, 461 (2009).
[2]T. A. Schmidt, N. S. Gastelum, Q. T. Nguyen, B. L. Schumacher, and R. L. Sah, Arthritis Rheum. **56**, 882 (2007).
[3]T. A. Schmidt and R. L. Sah, Osteoarthritis Cartilage **15**, 35 (2007).
[4]J. N. Katz, K. R. Arant, and R. F. Loeser, JAMA **325**, 568 (2021).
[5]C. R. Scanzello and S. R. Goldring, Bone **51**, 249 (2012).
[6]K. A. Esmonde-White, G. S. Mandair, F. Raaii, J. A. Jacobson, B. S. Miller, A. G. Urquhart, B. J. Roessler, and M. D. Morris, J. Biomed. Opt. **14**, 034013 (2009).
[7]A. Y. Hui, W. J. McCarty, K. Masuda, G. S. Firestein, and R. L. Sah, WIREs Syst. Biol. Med. **4**, 15 (2012).
[8]M. Daniel, Wien. Med. Wochenschr. **164**, 88 (2014).
[9]W. Lin and J. Klein, Adv. Mater. **33**, 2005513 (2021).
[10]T. Murakami, K. Nakashima, S. Yarimitsu, Y. Sawae, and N. Sakai, Proc. Inst. Mech. Eng., Part J: J. Eng. Tribol. **225**, 1174 (2011).
[11]S. M. T. Chan, C. P. Neu, G. Duraine, K. Komvopoulos, and A. H. Reddi, Osteoarthritis Cartilage **18**, 956 (2010).
[12]Y. Duan, Y. Liu, C. Zhang, Z. Chen, and S. Wen, Langmuir **32**, 10957 (2016).
[13]L. Zhu, J. Seror, A. J. Day, N. Kampf, and J. Klein, Acta Biomater. **59**, 283 (2017).
[14]Z. Pawlak, W. Urbaniak, and A. Oloyede, *Biomaterials and Medical Tribology* (Elsevier, Amsterdam, The Netherland, 2013), p. 253.
[15]Z. Pawlaka, A. Gadomskic, M. Hagner-Derengowskab, and W. U. P. Bełdowskic, "A lamellar–repulsive mechanism of lubrication of natural joints," in *STLE Annual Meeting & Exhibition*, Dallas, TX, 17–21 May 2015 (STLE, 2015).
[16]W. Lin, Z. Liu, N. Kampf, and J. Klein, Cells **9**, 1606 (2020).
[17]M. Herzog, L. Li, H.-J. Galla, and R. Winter, Colloids Surf. B: Biointerfaces **173**, 327 (2019).
[18]D. C. F. Wieland, P. Degen, T. Zander, S. Gayer, A. Raj, J. An, A. Dedinaite, P. Claesson, and R. Willumeit-Romer, Soft Matter **12**, 729 (2016).
[19]P. Smith, R. M. Ziolek, E. Gazzarrini, D. M. Owen, and C. D. Lorenz, Phys. Chem. Chem. Phys. **21**, 9845 (2019).
[20]J. R. Watterson and J. M. Esdaile, J. Am. Acad. Orthoped. Surg. **8**, 277 (2000).
[21]L. W. Moreland, Arthritis Res. Ther. **5**, 54 (2003).
[22]J.-P. Colletier *et al.*, BMC Biotechnol. **2**, 9 (2002).
[23]J. K. Zhao, C. Y. Gao, and D. Liu, J. Appl. Crystallogr. **43**, 1068 (2010).
[24]W. T. Heller *et al.*, J. Appl. Crystallogr. **51**, 242 (2018).
[25]G. T. Wignall and F. Bates, J. Appl. Crystallogr. **20**, 28 (1987).
[26]O. Arnold *et al.*, Nucl. Instrum. Methods Phys. Res. Sect. A **764**, 156 (2014).
[27]M. Agamalian, L. Heroux, K. Littrell, and J. Carpenter, in *22nd Meeting of the International Collaboration on Advanced Neutron Sources (ICANS XXII)*, Oxford, UK, 27-31 March 2017 (IOP Publishing, 2017), p. 012033.
[28]J. A. Lake, Acta Crystallogr. **23**, 191 (1967).
[29]J. Chappuis, I. A. Sherman, and A. W. Neumann, Ann. Biomed. Eng. **11**, 435 (1983).
[30]A. Mrela and Z. Pawlak, Biomed. J. Sci. Tech. Res. **6**, 5492 (2018).
[31]G. Wang, M. Rodahl, M. Edvardsson, S. Svedhem, G. Ohlsson, F. Hook, and B. Kasemo, Rev. Sci. Instrum. **79**, 075107 (2008).
[32]G. Duner, E. Thormann, and A. Dedinaite, J. Colloid Interface Sci. **408**, 229 (2013).
[33]G. Ohlsson, A. Tigerström, F. Höök, and B. Kasemo, Soft Matter **7**, 10749 (2011).
[34]V. Nele, M. N. Holme, U. Kauscher, M. R. Thomas, J. J. Doutch, and M. M. Stevens, Langmuir **35**, 6064 (2019).
[35]H. Schmiedel, L. Almasy, and G. Klose, Eur. Biophys. J. **35**, 181 (2006).
[36]S. Qian, V. K. Sharma, and L. A. Clifton, Langmuir **36**, 15189 (2020).
[37]E. Geissler, A. M. Hecht, and F. Horkay, in *Macromolecular Symposia* (Wiley Online Library, New York, 2010), Vol. 291–292, Issue 1, pp. 362–370.
[38]R. Mendichi, L. Soltes, and A. Giacometti Schieroni, Biomacromolecules **4**, 1805 (2003).
[39]D.-M. Smilgies and E. Folta-Stogniew, J. Appl. Crystallogr. **48**, 1604 (2015).
[40]B. Nystrom, A.-L. Kjoniksen, N. Beheshti, A. Maleki, K. Zhu, K. D. Knudsen, R. Pamies, J. G. Hernandez Cifre, and J. Garcia de la Torre, Adv. Colloid Interface Sci. **158**, 108 (2010).
[41]B. Seantier, C. Breffa, O. Felix, and G. Decher, J. Phys. Chem. B **109**, 21755 (2005).
[42]J.-H. Choi, S.-O. Kim, E. Linardy, E. C. Dreaden, V. P. Zhdanov, P. T. Hammond, and N.-J. Cho, J. Colloid Interface Sci. **448**, 197 (2015).
[43]J. E. Scott and F. Heatley, Proc. Natl. Acad. Sci. U.S.A. **96**, 4850 (1999).
[44]N. M. Elayan, W. D. Treleaven, and R. L. Cook, Environ. Sci. Technol. **42**, 1531 (2008).
[45]A. Taglienti, F. Cellesi, V. Crescenzi, P. Sequi, M. Valentini, and N. Tirelli, Macromol. Biosci. **6**, 611 (2006).
[46]T. Zander, V. M. Garamus, A. Dedinaite, P. M. Claesson, P. Beldowski, K. Gorny, Z. Dendzik, D. C. F. Wieland, and R. Willumeit-Romer, Molecules **25**, 3907 (2020).
[47]R.-H. Mikelsaar and J. E. Scott, Glycoconj. J. **11**, 65 (1994).
[48]T. Zander *et al.*, Colloids Surf. B: Biointerfaces **142**, 230 (2016).
[49]J. Siodmiak, P. Beldowski, W. Auge, D. Ledzinski, S. Smigiel, and A. Gadomski, Molecules **22**, 1436 (2017).
[50]P. Beldowski, S. Yuvan, A. Dedinaite, P. M. Claesson, and T. Poschel, Colloids Surf B: Biointerfaces **184**, 110539 (2019).
[51]A. Dėdinaitė, D. C. F. Wieland, P. Bełdowski, and P. M. Claesson, Adv. Colloid Interface Sci. **274**, 102050 (2019).
[52]A. Kolarikova, E. Kutalkova, V. Bus, R. Witasek, J. Hrncirik, and M. Ingr, Carbohydr. Polym. **286**, 119288 (2022).
[53]L. Beney, J. M. Perrier-Cornet, M. Hayert, and P. Gervais, Biophys. J. **72**, 1258 (1997).
[54]J.-M. Perrier-Cornet, K. Baddouj, and P. Gervais, J. Membr. Biol. **204**, 101 (2005).
[55]Y. Li, S. Ruan, Z. Wang, N. Feng, and Y. Zhang, Pharmaceutics **13**, 1235 (2021).
[56]R. Ionov, A. El-Abed, M. Goldmann, and P. Peretti, Biochim. Biophys. Acta (BBA)-Biomembr. **1667**, 200 (2004).
[57]M. Kreuzer, M. Strobl, M. Reinhardt, M. C. Hemmer, T. Hauss, R. Dahint, and R. Steitz, Biochim. Biophys. Acta (BBA)-Biomembr. **1818**, 2648 (2012).
[58]T. L. Nascimento *et al.*, Langmuir **31**, 11186 (2015).
[59]H. Sahoo and P. Schwille, Soft Matter **9**, 3859 (2013).
[60]R. Crockett, A. Grubelnik, S. Roos, C. Dora, W. Born, and H. Troxler, J. Biomed. Mater. Res. Part A **82A**, 958 (2007).
[61]R. Sorkin, Y. Dror, N. Kampf, and J. Klein, Langmuir **30**, 5005 (2014).
[62]E. A. Balazs, D. Watson, I. F. Duff, and S. Roseman, Arthritis Rheum. **10**, 357 (1967).
[63]S. Graindorge, W. Ferrandez, E. Ingham, Z. Jin, P. Twigg, and J. Fisher, Proc. Inst. Mech. Eng. Part H: J. Eng. Med. **220**, 597 (2006).
[64]S. Graindorge, W. Ferrandez, Z. Jin, E. Ingham, C. Grant, P. Twigg, and J. Fisher, Med. Eng. Phys. **27**, 836 (2005).
[65]S. Jahn, J. Seror, and J. Klein, Annu. Rev. Biomed. Eng. **18**, 235 (2016).
[66]See supplementary material at https://www.scitation.org/doi/suppl/10.1116/6.0002502 for details about the model to fit SANS spectra, DLS measurements of the reference samples, QCM and AFM results for the reference samples, and AFM cross sections of the films.

13 May 2024 08:52:55

© Author(s) 2023